

Structural Remodeling of Active Zones Is Associated with Synaptic Homeostasis

Huilin Hong,^{1,2} Kai Zhao,¹ Shiyuan Huang,¹ Sheng Huang,³ Aiyu Yao,¹ Yuqiang Jiang,¹ Stephan Sigrist,³  Lu Zhao,⁴ and  Yong Q. Zhang^{1,2}

¹State Key Laboratory for Molecular and Developmental Biology, CAS Center for Excellence in Brain Science and Intelligence Technology, Institute of Genetics and Developmental Biology, Chinese Academy of Sciences, Beijing, 10010, China, ²University of Chinese Academy of Sciences, Beijing, 100049, China, ³Freie Universität Berlin, Institute for Biology, 14195 Berlin, Germany, and ⁴Yunnan Key Laboratory of Primate Biomedical Research, Institute of Primate Translational Medicine, Kunming University of Science and Technology, Kunming, 650500, China

Perturbations to postsynaptic glutamate receptors (GluRs) trigger retrograde signaling to precisely increase presynaptic neurotransmitter release, maintaining stable levels of synaptic strength, a process referred to as homeostatic regulation. However, the structural change of homeostatic regulation remains poorly defined. At wild-type *Drosophila* neuromuscular junction synapse, there is one Bruchpilot (Brp) ring detected by superresolution microscopy at active zones (AZs). In the present study, we report multiple Brp rings (i.e., multiple T-bars seen by electron microscopy) at AZs of both male and female larvae when GluRs are reduced. At *GluRIIC*-deficient neuromuscular junctions, quantal size was reduced but quantal content was increased, indicative of homeostatic presynaptic potentiation. Consistently, multiple Brp rings at AZs were observed in the two classic synaptic homeostasis models (i.e., *GluRIIA* mutant and pharmacological blockade of *GluRIIA* activity). Furthermore, postsynaptic overexpression of the cell adhesion protein Neuroligin 1 partially rescued multiple Brp rings phenotype. Our study thus supports that the formation of multiple Brp rings at AZs might be a structural basis for synaptic homeostasis.

Key words: active zone; GluRs; homeostatic regulation; Neuroligin 1; structural remodeling

Significance Statement

Synaptic homeostasis is a conserved fundamental mechanism to maintain efficient neurotransmission of neural networks. Active zones (AZs) are characterized by an electron-dense cytomatrix, which is largely composed of Bruchpilot (Brp) at the *Drosophila* neuromuscular junction synapses. It is not clear how the structure of AZs changes during homeostatic regulation. To address this question, we examined the structure of AZs by superresolution microscopy and electron microscopy during homeostatic regulation. Our results reveal multiple Brp rings at AZs of glutamate receptor-deficient neuromuscular junction synapses compared with single Brp ring at AZs in wild type (WT). We further show that Neuroligin 1-mediated retrograde signaling regulates multiple Brp ring formation at glutamate receptor-deficient synapses. This study thus reveals a regulatory mechanism for synaptic homeostasis.

Introduction

Synaptic connections undergo homeostatic readjustment in response to changes of synaptic activity, to ensure a flexible yet

stable nervous system. Compelling evidence has shown that homeostatic signaling acts in both the central and peripheral nervous systems in various species ranging from *Drosophila* to humans (Pozo and Goda, 2010; Turrigiano, 2012; Davis and Müller, 2015). For example, reduced postsynaptic sensitivity at endplates of myasthenia gravis patients is counteracted by upregulated neurotransmitter release to restore evoked postsynaptic current amplitudes and maintain muscle excitation (Cull-Candy et al., 1980). Studies in rodents also reported that partial blockage of acetylcholine receptors triggers a compensatory increase in presynaptic release (Wang et al., 2010, 2016). Extensive studies at *Drosophila* neuromuscular junctions (NMJs) have uncovered molecular mechanisms underlying this homeostatic regulation (e.g., with

Received Aug. 17, 2019; revised Feb. 16, 2020; accepted Feb. 22, 2020.

Author contributions: H.H., L.Z., and Y.Q.Z. designed research; H.H. and K.Z. performed research; H.H., K.Z., Shiyuan Huang, Sheng Huang, A.Y., Y.J., S.S., L.Z., and Y.Q.Z. analyzed data; H.H. and Y.Q.Z. wrote the paper.

This work was supported by Ministry of Science and Technology Grant 2016YFA0501000, and National Science Foundation of China Grant 31490590 to Y.Q.Z. and Grant 3140060310 to L.Z. We thank Thomas Schwarz for discussion; Aron DiAntonio, Troy Littleton, Bloomington Stock Center, Tshinghua RNAi Stock Center, VDRC Stock Center, and the Developmental Studies Hybridoma Bank for providing fly stocks and antibodies.

The authors declare no competing financial interests.

Correspondence should be addressed to Yong Q. Zhang at yqzhang@genetics.ac.cn or Lu Zhao at zhaol@pbr.cn.

<https://doi.org/10.1523/JNEUROSCI.2002-19.2020>

Copyright © 2020 the authors

an increase of presynaptic vesicle (pre-SV) release being mediated via an increase of action potential associated calcium influx and changed kinetics of vesicle recruitment) (Frank et al., 2006; Müller et al., 2011; Davis and Müller, 2015). Thus, presynaptic release could be functionally adjusted in homeostasis. Whether and how structural changes at presynapses occur to promote increases at presynaptic release sites during homeostatic regulation is a critical but still insufficiently addressed question.

The active zone (AZ) is a specialized structure of presynaptic release sites, which mediates neurotransmitter release and consists of an evolutionarily conserved protein complex, including Bruchpilot (Brp), RIM-binding-protein (RBP), and Syd-1 (synapse defective 1) (Dai et al., 2006; Kittel et al., 2006; Fouquet et al., 2009; Oswald et al., 2010; Liu et al., 2011). Brp is a key component of the electron-dense projection T-bar at AZs, and loss of Brp provokes severe deficits in AZ assembly of *Drosophila* NMJ synapses (Kittel et al., 2006; Wagh et al., 2006; Fouquet et al., 2009). During development, the molecular complexity and Brp content of AZ increase with enhanced synaptic strength (Peled et al., 2014), indicating structural modification during synaptic maturation. AZ structural remodeling also occurs during synaptic plasticity. In visual systems of flies and mice, light-dark changes have been shown to affect the AZ structure of photoreceptors (Spiwoks-Becker et al., 2004; Sugie et al., 2015). Recent superresolution light microscopy has revealed an enlargement of Brp-positive AZs upon synaptic homeostasis induction (Weyhersmüller et al., 2011; Böhme et al., 2019; Goel et al., 2019; Gratz et al., 2019), suggesting that the structural reorganization of AZ may also contribute to the homeostatic regulation of synapses. However, the mechanism by which these structural changes occur at presynaptic release sites during presynaptic homeostatic potentiation (PHP) remains unclear.

Although several retrograde signaling pathways are involved in PHP (Haghighi et al., 2003; McCabe et al., 2003; Goold and Davis, 2007; Pilgram et al., 2011; Penney et al., 2012), a clear picture of how homeostatic plasticity is regulated from the postsynaptic to presynaptic sides has not yet to emerge. Transsynaptic cell adhesion molecules, such as neuroligin (Nrx)-neuroligin (Nlg) and terneurins, have been shown to mediate coordinated assembly of presynaptic and postsynaptic specializations and to control the proper alignment of AZs with postsynaptic receptors (Dalva et al., 2007; Li et al., 2007; Giagtzoglou et al., 2009; Banovic et al., 2010; Mosca et al., 2012). However, it is not known whether cell adhesion molecules mediate the retrograde signal for PHP (Pozo and Goda, 2010).

Using confocal, superresolution structured illumination microscopy (SIM) and electron microscopy, we found that clusters of multiple Brp rings were induced after genetic reduction of postsynaptic glutamate receptor. Multiple Brp rings at a single AZ were also detected at NMJ synapses of *GluRIIA* mutants and PhTx (Philanthotoxin-433, a glutamate receptor blocker)-treated animals, both of which exhibit robust and well-studied PHP. Thus, the formation of multiple Brp rings might be the presynaptic structural basis for PHP. We further found that the cell adhesion molecule, Nlg1, was involved in the retrograde regulation of multiple Brp ring formation. Together, our findings revealed distinct restructuring of presynaptic AZs upon postsynaptic GluR reduction-induced synaptic homeostasis.

Materials and Methods

Drosophila stocks and husbandry. All fly stocks of both males and females were, if not otherwise stated, raised on standard cornmeal medium at 25°C and 65% humidity. The *w¹¹¹⁸* flies were used as WT controls unless otherwise specified. *UAS-GluRIIC RNAi* (THU2586) was from Tsinghua

University *Drosophila* Stock Center (<http://fly.redbux.cn>). The muscle-specific *C57-Gal4* was from Bloomington Fly Stock Center. *GluRIIC* mutant lines *GluRIIC²/CyO-GFP* and *Dfast2/CyO-GFP;UAS-cGluRIIC/TM6B*, *GluRIIC* rescue line *Dfast2/CyO-GFP;UAS-gGluRIIC/TM6B*, *GluRIIA* mutant alleles *DfCl^{h4}/CyO-GFP* and *GluRIIA^{AD9}/CyO-GFP*, and *MHC-IIIB* were obtained from Dr. A. DiAntonio (Petersen et al., 1997; Marrus and DiAntonio, 2004). *UAS-nlg1-GFP* was a gift from Dr. T. Littleton (Harris et al., 2016). *GluRIIA^{GFP}* (GluRIIA carrying GFP at its C terminus), *Cac-sfGFP/FM7a*, and *nlg1* mutant alleles *nlg1^{ex2.3}* and *nlg1^{ex1.9}* were described previously (Rasse et al., 2005; Banovic et al., 2010; Gratz et al., 2019).

Immunochemical analysis and imaging. Immunostaining of larval neuromuscular structures was performed as previously described (Zhao et al., 2013). For immunostaining involving antibodies against glutamate receptors and for structural illumination microscopy imaging, samples were fixed with ice-cold methanol for 10 min. For staining with antibodies against other proteins, samples were fixed in 4% PFA for 45 min. Mouse monoclonal anti-Brp (Nc82, 1:50), anti-GluRIIA (8B4D2, 1:1000) were from the Developmental Studies Hybridoma Bank (University of Iowa, Iowa City, IA). Chicken polyclonal antibody to GFP was from Abcam (ab13970, 1:500). Rabbit polyclonal antibody against GluRIIB (1:2500) was from Dr. A. DiAntonio (Marrus and DiAntonio, 2004). Rabbit polyclonal anti-GluRIID (1:2500), guinea pig anti-RBP (1:1000), rabbit anti-Syd-1 (1:1000), and rabbit polyclonal anti-Nlg1 (1:1000) were described previously (Qin et al., 2005; Li et al., 2007; Banovic et al., 2010; Matkovic et al., 2013; Ullrich et al., 2015). Anti-HRP conjugated with FITC or Texas Red (1:100) was from Jackson ImmunoResearch Laboratories. Secondary antibodies, including Alexa 488-, 568-, or 647-conjugated anti-mouse, anti-rabbit, anti-guinea pig, and anti-chicken IgG (1:1000), were obtained from Invitrogen. All images of muscle 4 NMJ (NMJ4) from abdominal segments A2 or A3 for a specific experiment were captured using identical settings for statistical comparison among different genotypes.

Conventional confocal images were collected with a Fluoview FV1000 confocal microscope (Olympus) using a 60× oil objective (numerical aperture: 1.42). Confocal stacks were processed with ImageJ software (National Institutes of Health). The signal of anti-HRP staining was used to outline the area of NMJ terminals for quantitative analysis. For the measurement of Brp staining intensity and puncta size, we collected images with identical settings across different genotypes for a given experiment. Although most Brp puncta were distinct, occasional overlapping puncta were separated with the cut drawing tool. Superresolution images were obtained with an SIM (Delta Vision OMX V4; GE Healthcare) using a 60× oil objective (NA 1.42; Olympus). Raw data were reconstructed with softWoRx 6.5.2 (GE Healthcare). Default reconstruction parameters were applied. Images for figures were processed with Imaris 6.0 software (<http://www.bitplane.com>).

PhTx treatment. The glutamate receptor blocker PhTx (Sigma Millipore) was prepared as a 1 mM stock solution in DMSO (Sigma Millipore) and diluted in HL3.1 to final concentrations of 200 and 10 μM. For verification of PhTx efficacy, PhTx (200 μM) was injected into the abdominal cavity of third instar WT larvae using a glass microelectrode. For acute treatment, semi-intact WT larvae were incubated with 10 μM PhTx for 10 min or 30 min. Controls were treated with HL3.1 containing the DMSO vehicle as in the experimental group.

Electron microscopy. Tissue for electron microscopy experiments was prepared as previously described (Zhao et al., 2013). Images were captured on a JEOL 1400 transmission electron microscope equipped with a Ganton 792 CCD using 80 kV accelerating voltage. Electron micrographs of NMJs were taken from muscles 6/7 of segments A3–A4 in four larvae of each genotype. Image magnifications ranged from 30,000 to 80,000 to allow visualization of structures ranging in size from an entire bouton to a single AZ. ImageJ software was used to measure bouton perimeters and AZ lengths. High-magnification images (80,000×) were used to determine the T-bar parameters, which was defined as an electron-dense rod surrounded by vesicles and adjacent to the presynaptic membrane. The length of electron densities found between presynaptic and postsynaptic membranes was also statistically analyzed.

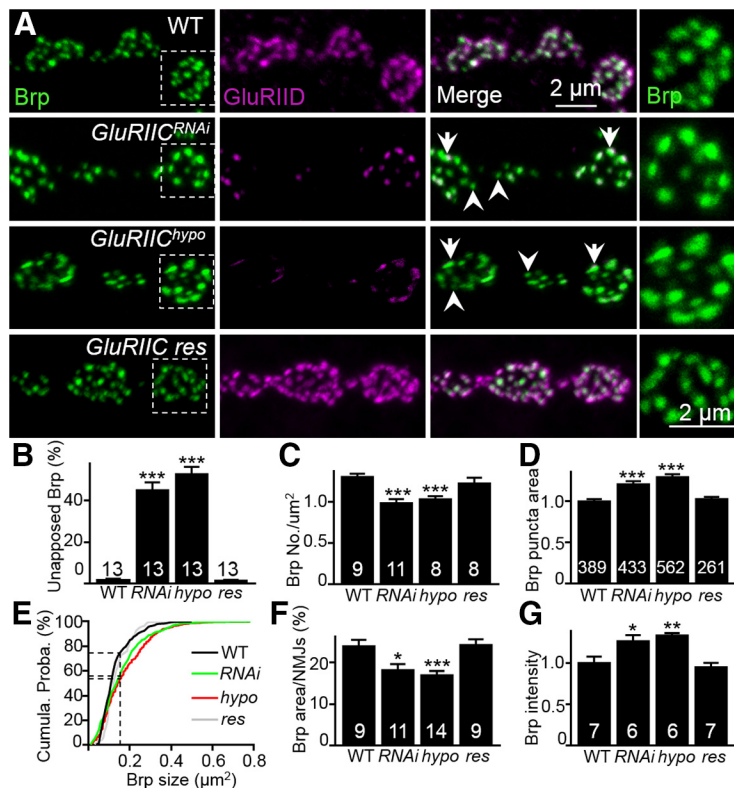


Figure 1. NMJ boutons contain fewer and larger Brp puncta when postsynaptic GluRs are reduced. **A**, Confocal images of muscle 4 NMJ stained with anti-Brp (green) and anti-GluRIID (magenta) from WT (w^{1118}), $GluRIIC^{RNAi}$ ($C57-Gal4/GluRIIC^{RNAi}$), $GluRIIC^{hypo}$ mutant ($GluRIIC^2/Dfast2; UAS-GluRIIC/+$), and $GluRIIC^{res}$ ($GluRIIC^2/Dfast2; gGluRIIC/+$). Arrowheads indicate Brp puncta without opposing GluRIID. Arrows indicate Brp puncta with juxtaposed GluRIID. Scale bar, 2 μm . Left column, The enlarged views of the boxed area. Scale bar, 1 μm . **B**, The percentage of Brp puncta unapposed to GluRIID in different genotypes (WT, $GluRIIC^{RNAi}$, $GluRIIC^{hypo}$, and $GluRIIC^{res}$). $n = 13$ boutons for each genotype. **C, D**, Bar graphs represent the number of Brp puncta per μm^2 of NMJ (**C**) and normalized Brp puncta area (**D**) in different genotypes. Error bars indicate stand error of mean (SEM). $***p < 0.001$. **E**, Cumulative probability plot of Brp puncta size at NMJ synapses of WT, $GluRIIC^{RNAi}$, $GluRIIC^{hypo}$, and $GluRIIC^{res}$. **F, G**, Quantification of Brp area (**F**) and Brp intensity (**G**) at the NMJs of different genotypes. $*p < 0.05$, $**p < 0.01$, $***p < 0.001$. Error bars indicate SEM. For staining of other AZ markers at $GluRIIC$ mutant NMJs, see also Figure 1-1 (available at <https://doi.org/10.1523/JNEUROSCI.2002-19.2020.f1-1>).

Electrophysiology. Electrophysiological experiments were performed as previously described with minor modifications (Zhao et al., 2013). Third-instar larvae were dissected in HL-3.1 saline (Ca^{2+} free), then washed with and recorded in HL-3.1 saline containing different concentrations of Ca^{2+} (0.3, 1.0, and 1.5 mM). Intracellular microelectrodes with a resistance $>5 M\Omega$ filled with 3 M KCl were used for the assay. Excitatory junctional potentials (EJPs) and miniature EJPs (mEJPs) were recorded from muscle 6 in segments A3 and A4 for 100 s. EJPs were elicited by low-frequency (0.3 Hz) stimulation. We analyzed recordings from muscle cells with physiological resting potentials ≤ -60 mV and input resistances $> 5 M\Omega$.

Statistical analyses. Statistical significance between a specific genotype and the control was determined by two-tailed Student's t test, whereas multiple comparison between genotypes was determined by one-way ANOVA with a Tukey *post hoc* test and two-way ANOVA. Asterisks above a column indicate comparisons between a specific genotype and control, whereas asterisks above a horizontal line denote comparisons between two specific genotypes.

Results

Presynaptic Brp puncta are enlarged at GluR-deficient NMJ synapses

The fly NMJ GluRs are heterotetrameric complexes composed of three essential subunits (GluRIIC, GluRIID, and GluRIIE) and either GluRIIA or GluRIIB. Loss of any one of the essential GluR subunits leads to the absence of GluRs and embryonic lethality, whereas

loss of either GluRIIA or GluRIIB does not affect viability (Petersen et al., 1997; DiAntonio et al., 1999; Marrus et al., 2004; Featherstone et al., 2005; Qin et al., 2005). To investigate whether AZ structures changed when postsynaptic GluRs were reduced, we examined NMJ synapses of third-instar larvae of WT and $GluRIIC$ mutant animals. We costained NMJ terminals for the presynaptic AZ protein Brp and the essential GluR subunit GluRIID. As expected, we observed a severe reduction of GluRs in the muscle-specific $GluRIIC$ knockdown (hereafter $GluRIIC^{RNAi}$) and hypomorphic $GluRIIC$ mutants (hereafter $GluRIIC^{hypo}$) compared with WT synapses (Fig. 1A). The residual receptors still preferentially clustered opposite a subgroup of AZs as in WT (Fig. 1A, arrows) while leaving approximately half of AZs unopposed to receptors (Fig. 1A, arrowheads; Fig. 1B; $GluRIIC^{RNAi}$: $p < 0.001$, $t_{(24)} = 11.39$; $GluRIIC^{hypo}$: $p < 0.001$, $t_{(24)} = 14.48$).

We statistically analyzed the number and size of Brp puncta throughout NMJ4 terminals. We found that the number of Brp puncta at NMJ boutons was significantly reduced in $GluRIIC^{RNAi}$ and $GluRIIC^{hypo}$ mutants compared with WT (Fig. 1C; $GluRIIC^{RNAi}$: $p < 0.001$, $t_{(18)} = 4.90$; $GluRIIC^{hypo}$: $p < 0.001$, $t_{(15)} = 4.82$). However, the relative size of individual Brp puncta was increased significantly when $GluRIIC$ was reduced (Fig. 1D; $GluRIIC^{RNAi}$: $p < 0.001$, $t_{(820)} = 4.21$; $GluRIIC^{hypo}$: $p < 0.001$, $t_{(949)} = 6.00$). The cumulative probability plots of single Brp puncta size distributions showed that only

25% Brp puncta were $> 0.18 \mu m^2$ in the WT, whereas 42% and 48% Brp puncta were $> 0.18 \mu m^2$ in $GluRIIC^{RNAi}$ and $GluRIIC^{hypo}$ mutant boutons, respectively (Fig. 1E). It is also worth noting that Brp puncta $> 0.6 \mu m^2$ presented in $GluRIIC^{RNAi}$ and $GluRIIC^{hypo}$ mutants were never observed in WT (Fig. 1E). Furthermore, we observed a reduced Brp area (Fig. 1F; $GluRIIC^{RNAi}$: $p = 0.0163$, $t_{(18)} = 2.65$; $GluRIIC^{hypo}$: $p = 0.0009$, $t_{(21)} = 6.00$) and an increased intensity of Brp puncta (Fig. 1G; $GluRIIC^{RNAi}$: $p = 0.0364$, $t_{(11)} = 3.88$; $GluRIIC^{hypo}$: $p = 0.0034$, $t_{(11)} = 3.72$) in $GluRIIC$ RNAi knockdown and $GluRIIC^{hypo}$ mutant NMJs compared with WT. Expression of $GluRIIC$ from a single copy of the genomic transgene in $GluRIIC^{hypo}$ mutants ($GluRIIC^2/Dfast2; UAS-gGluRIIC/+$, named $GluRIIC^{res}$ thereafter) fully rescued the fewer but enlarged Brp puncta phenotype (Fig. 1A–D) as well as the increased area and intensity of Brp staining (Fig. 1F, G), demonstrating that the presynaptic Brp phenotype was indeed caused by the reduction of postsynaptic GluRIIC.

The enlarged Brp puncta and increased Brp intensity in $GluRIIC$ -deficient synapses suggest that the AZ size could be increased. To further address this possibility, we performed costaining of Brp with other AZ scaffolding proteins RBP and Syd-1 of both WT and $GluRIIC$ mutant NMJs. RBP directly interacts with calcium channels and regulates calcium channel po-

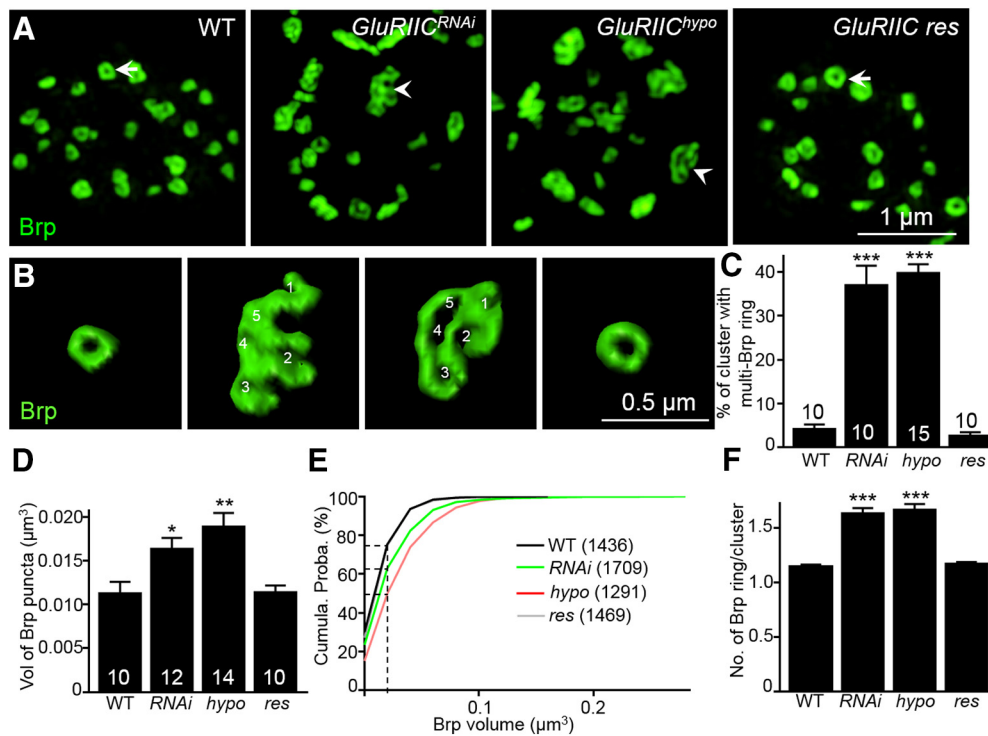


Figure 2. Multiple Brp rings cluster together in *GluRIIC^{RNAi}* and *GluRIIC^{hypo}* mutants. **A**, Superresolution images of NMJ boutons of WT, *GluRIIC^{RNAi}*, *GluRIIC^{hypo}*, and *GluRIIC^{res}* larvae stained with anti-Brp (green). Arrows indicate a single Brp ring. Arrowheads indicate multiple Brp rings. Scale bar, 1 μm . **B**, Three-dimensional reconstruction images of a single synapse indicated by arrows and arrowheads in **A**. Scale bar, 0.5 μm . **C**, Statistics of the percentage of multiple Brp rings at NMJ boutons in WT, *GluRIIC^{RNAi}*, *GluRIIC^{hypo}*, and *GluRIIC^{res}*. *n* values are indicated in the columns. **D**, Quantification of Brp puncta volume in different genotypes. When *GluRIIC* is reduced, Brp volume increases compared with WT. **E**, Cumulative probability plot of Brp puncta volume at NMJ boutons of WT, *GluRIIC^{RNAi}*, *GluRIIC^{hypo}*, and *GluRIIC^{res}*. **F**, Quantification of Brp ring numbers per Brp cluster at NMJ boutons of WT, *GluRIIC^{RNAi}*, *GluRIIC^{hypo}*, and *GluRIIC^{res}*. *n* = 8. Error bars indicate SEM. * p < 0.05, ** p < 0.01, *** p < 0.001.

sitioning at presynaptic AZs; Syd-1 is involved in promoting Brp clustering and AZ assembly at *Drosophila* AZs (Owald et al., 2010; Liu et al., 2011). As with Brp, the staining intensity and puncta size of RBP and Syd-1 in *GluRIIC^{RNAi}* (RBP intensity: p < 0.001, $t_{(10)} = 16.74$; RBP size: p < 0.001, $t_{(380)} = 9.56$; Syd-1 intensity: $p = 0.077$, $t_{(6)} = 2.14$; Syd-1 size: $p = 0.0184$, $t_{(164)} = 2.382$) and *GluRIIC^{hypo}* mutant (RBP intensity: p < 0.001, $t_{(10)} = 14.39$; RBP size: p < 0.001, $t_{(425)} = 12.23$; Syd-1 intensity: $p = 0.0295$, $t_{(6)} = 2.843$; Syd-1 size: $p = 0.0524$, $t_{(220)} = 1.951$) NMJs were increased compared with those in the WT (Fig. 1-1A–D, available at <https://doi.org/10.1523/JNEUROSCI.2002-19.2020.f1-1>). Again, expression of *GluRIIC* from a single copy of genomic *GluRIIC* in *GluRIIC^{hypo}* mutants rescued the enlarged RBP and Syd-1 puncta (Fig. 1-1A–D, available at <https://doi.org/10.1523/JNEUROSCI.2002-19.2020.f1-1>). Together, these results showed that presynaptic AZ scaffold sizes increased in response to a reduction of postsynaptic GluRs.

Superresolution imaging reveals clusters of Brp rings at *GluRIIC* mutant synapses

The fine architectures of AZs at nanometer scale are far beyond the resolution limit of conventional light microscopes. To further define the structural abnormalities of AZs at *GluRIIC* mutant synapses, we performed superresolution SIM on NMJ synapses. The lateral resolution is 250 nm for conventional microscopy while the lateral resolution is ~ 120 nm for SIM (Gustafsson et al., 2008). Consistent with a previous report (Kittel et al., 2006), we observed that Brp detected by the antibody Nc82 against a C-terminal epitope formed ring-like structures at WT NMJs (Fig. 2A, B, arrow), with an average volume of $0.011 \pm 0.001 \mu\text{m}^3$ (Fig.

2D). In *GluRIIC* mutants, the average volume of Brp puncta was significantly increased (Fig. 2D, E; $p = 0.0104$, $t_{(20)} = 2.828$ for *GluRIIC^{RNAi}*; $p = 0.0020$, $t_{(22)} = 3.50$ for *GluRIIC^{hypo}*), consistent with the increased Brp puncta observed by confocal microscopy (Fig. 1A). Superresolution images revealed that 37% and 40% of Brp clusters contained multiple Brp rings (two or more rings) in *GluRIIC^{RNAi}* and *GluRIIC^{hypo}* mutant NMJs, respectively, compared with only 4.2% in WT (Fig. 2A–C). The number of Brp ring per Brp cluster was increased from 1.14 ± 0.014 in WT to 1.65 ± 0.050 (p < 0.001, $t_{(14)} = 9.742$) in *GluRIIC^{RNAi}* and to 1.67 ± 0.053 (p < 0.001, $t_{(14)} = 9.554$) in *GluRIIC^{hypo}* mutant NMJ boutons (Fig. 2F). The multiple Brp ring phenotype in *GluRIIC^{hypo}* mutants was fully rescued by a single copy of genomic *GluRIIC* (Fig. 2C). Together, the SIM imaging results demonstrated that reduced GluRs led to formation of clusters of multiple Brp rings at AZs of NMJ synapses.

Ultrastructural analysis reveals multiple T-bars at the AZs of GluR-deficient synapses

AZs at *Drosophila* NMJ synapses are recognized by electron-dense membranes and an electron-dense cytomatrix, which is largely composed of Brp and called “T-bar” due to its morphology (Zhai and Bellen, 2004; Fouquet et al., 2009). To determine whether AZ ultrastructure was affected in *GluR* mutants, we performed electron microscopy analysis and observed no difference in the bouton perimeter between WT and *GluRIIC^{hypo}* mutant animals (Fig. 3A, B; $p = 0.132$, $t_{(129)} = 1.514$). However, the length of electron-dense membranes in *GluRIIC^{hypo}* mutants was significantly shorter than that in the WT (Fig. 3C, D; WT: $0.72 \pm 0.025 \mu\text{m}$, *GluRIIC^{hypo}*: $0.39 \pm 0.027 \mu\text{m}$, p < 0.001, $t_{(129)} =$

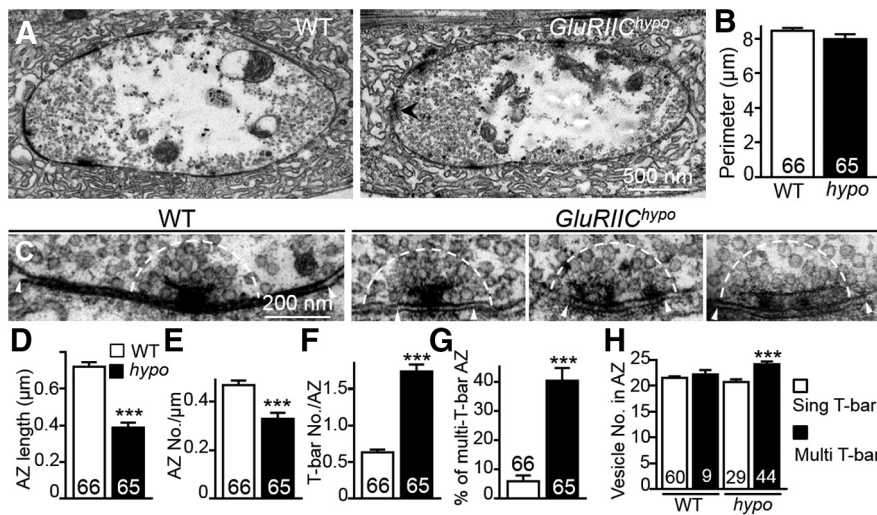


Figure 3. There are multiple T-bars in AZs when *GluRIIC* is reduced. **A**, A cross section of WT and *GluRIIC^{hypo}* mutant boutons of M6/7 NMJs. Black arrowhead indicates the multiple T-bar AZ. Scale bar, 500 nm. **B**, Quantification of bouton perimeter in WT and *GluRIIC^{hypo}* mutants. **C**, Sections of representative AZs from WT and *GluRIIC^{hypo}* synapses. White arrowheads indicate the boundaries of electron densities. Scale bar, 200 nm. **D–H**, Quantification of electron density length (**D**), the number of AZs per μm of bouton perimeter (**E**), the average number of T-bars per AZ (**F**), the percentage of multiple T-bar AZs (**G**), and the number of SVs within a 200 nm radius of AZs indicated by dashed lines for WT and *GluRIIC^{hypo}* terminals (**H**). Error bars indicate SEM. ****p* < 0.001.

9.077). This reduction of the electron-dense membrane suggest a defect of cytomatrix protein assembly, which is important for the organization of AZs. At WT NMJs, the synaptic cleft was filled with electron-dense material arranged as a ladder-like scaffold of macromolecular complexes connecting the presynaptic and postsynaptic membranes. However, the ladder-like electron-dense material was greatly reduced leaving a largely empty cleft at *GluRIIC^{hypo}* mutant synapses (Fig. 3C), indicating that formation of the ladder like structure in synaptic cleft is dependent on GluRs.

Electron microscopy analysis also showed that the AZ number in *GluRIIC^{hypo}* was significantly reduced compared with that in the WT (Fig. 3E; WT: $0.47 \pm 0.018/\mu\text{m}$ bouton perimeter, *GluRIIC^{hypo}*: $0.33 \pm 0.025/\mu\text{m}$ bouton perimeter, *p* < 0.001, $t_{(129)} = 4.527$), consistent with fewer Brp puncta in *GluR* mutants (Fig. 1B). In contrast to the reduced number of AZs (i.e., Brp puncta), we found more T-bars at AZ in *GluRIIC^{hypo}* mutants compared with WT (Fig. 3F; WT: 0.63 ± 0.039 , *GluRIIC^{hypo}*: 1.74 ± 0.097 ; *p* < 0.001, $t_{(129)} = 10.68$); in addition, the percentage of AZs harboring multiple T-bars was higher in *GluRIIC^{hypo}* mutants than WT (Fig. 3G; WT: $6.04 \pm 2.00\%$, *GluRIIC^{hypo}*: $40.49 \pm 4.33\%$; *p* < 0.001, $t_{(129)} = 7.255$). We also found significantly more SVs within 200 nm of AZs with multiple T-bars in *GluRIIC^{hypo}* mutants compared with WT (*p* = 0.0003, $t_{(71)} = 3.853$), whereas single T-bar AZs in *GluRIIC^{hypo}* mutants contained a normal number of SVs as WT (Fig. 3H). Collectively, electron microscopy analysis revealed multiple T-bars at AZ associated with more SVs in *GluRIIC^{hypo}* mutant boutons, consistent with the multiple Brp rings observed by superresolution SIM microscopy.

***GluRIIC* mutant NMJs undergo functional homeostatic regulation**

As shown above, we found abnormal AZs with multiple T-bars at *GluRIIC* mutant NMJ boutons. How would these structural changes affect synaptic function? To answer this question, we performed electrophysiology at the third instar larval NMJs of both WT

and *GluRIIC* mutant animals (Fig. 4). Consistent with a previous report (Marrus and DiAntonio, 2004), we found reduced neurotransmission at *GluRIIC^{hypo}* mutant synapses (Fig. 4A). At physiological levels of external calcium of 1.5 mM, the *GluRIIC^{hypo}* mutant exhibited a reduced EJP amplitude (Fig. 4B; *p* < 0.001, $t_{(10)} = 21.49$) and reduced amplitude and frequency of spontaneous mEJP compared with WT (Fig. 4C,D; mEJP amplitude: *p* < 0.001, $t_{(12)} = 11.25$; mEJP frequency: *p* < 0.001, $t_{(12)} = 17.63$). The reduced amplitudes of evoked and spontaneous responses likely result from a reduction of glutamate receptors.

It is well established that presynaptic function is enhanced to maintain normal transmission strength at the *Drosophila* NMJ in response to reduced GluRIIA levels (Petersen et al., 1997; Davis and Goodman, 1998a). To assess whether pre-SV release was affected when the level of GluRIIC was reduced, we estimated the number of vesicles released per stimulus (i.e., quantal content [QC]), which is a

measure of synaptic transmission efficacy and is calculated by dividing the EJP amplitude (after correction for nonlinear summation) by the mEJP amplitude. We found that *GluRIIC^{hypo}* mutant synapses exhibited a significant increase in QC compared with WT at 1.5 mM Ca^{2+} (Fig. 4E; *p* = 0.0044, $t_{(10)} = 3.662$).

One possible explanation for the increased neurotransmitter release was a functional compensation for reduced postsynaptic receptors. Previous studies showed that the postsynaptic receptors preferentially clustered opposite high probability release sites (Marrus and DiAntonio, 2004; Graf et al., 2009). We supposed that, when evoked at physiological 1.5 mM Ca^{2+} , low probability release sites juxtaposing few receptors also fire, but exert a limited effect on the postsynaptic potential due to a limited amount of GluRs. Therefore, we investigated the synaptic transmission at a low external calcium level of 0.3 mM, with which only the high probability release sites were supposed to fire (Marrus and DiAntonio, 2004). We found that *GluRIIC^{hypo}* mutants showed a reduced spontaneous release but an increased QC at 0.3 mM Ca^{2+} (Fig. 4C, *p* = 0.0004, $t_{(13)} = 4.761$; Fig. 4D, *p* < 0.001, $t_{(16)} = 18.91$; Fig. 4E, *p* = 0.0063, $t_{(13)} = 3.252$). The low calcium level of 0.3 mM alleviated the reduction of EJP amplitude in *GluRIIC^{hypo}* mutants to a great extent (Fig. 4B; 18% reduction 0.3 mM calcium vs 57% reduction at 1.5 mM calcium of the WT EJP amplitude) so that the amplitude of EJP showed no significant reduction in *GluRIIC^{hypo}* mutants compared with WT (Fig. 4B; WT, 11.69 ± 0.85 mV vs *GluRIIC^{hypo}* mutant, 9.58 ± 0.57 mV, *p* = 0.1108, $t_{(18)} = 1.677$). Thus, the electrophysiological results showed homeostatic regulation at AZs with multiple T-bars at *GluRIIC* mutant NMJs.

Acute inhibition of GluR activity provokes formation of multiple Brp rings

GluR mutants or RNAi knockdown resulted in formation of multiple Brp rings at NMJ synapses. To examine whether blocking GluR activity could acutely lead to multiple Brp ring formation, we applied PhTx on semi-intact *Drosophila* larvae; PhTx blocks GluR activity within minutes and is assumed to specifically act on

GluRIIA at the *Drosophila* NMJ (Frank et al., 2006). To verify the efficacy of PhTx, we first applied 200 μ M PhTx onto wandering third-instar larvae as previously described (Frank et al., 2006) and found animals were immediately paralyzed testifying the efficacy of PhTx. We then examined Brp staining of semi-intact larvae treated with 10 μ M PhTx for 10 or 30 min and found that the Brp cluster size was enlarged at both time points (Fig. 5*A,B*; $p < 0.001$, $t_{(1818)} = 12.11$ for 10 min PhTx treatment; $p < 0.001$, $t_{(1963)} = 13.09$ for 30 min PhTx treatment). The mean intensity of Brp clusters was also significantly increased at both time points of PhTx treatments (Fig. 5*B*; $p = 0.003$, $t_{(30)} = 3.201$ for 10 min PhTx treatment; $p = 0.0004$, $t_{(32)} = 3.968$ for 30 min PhTx treatment). Together, these findings showed that acute inhibition of GluR activity induced an increase in both size and intensity of Brp puncta.

To further clarify whether increased Brp clustering following PhTx treatment was due to formation of multiple Brp rings similar to *GluRIIC* mutants, we imaged Brp staining by SIM and found enlarged Brp rings (Fig. 5*C,D*; vehicle control: ring diameter $0.19 \pm 0.006 \mu$ m; 10 min PhTx treatment: $0.24 \pm 0.006 \mu$ m, $p < 0.001$, $t_{(620)} = 5.802$; 30 min PhTx treatment: $0.25 \pm 0.006 \mu$ m, $p < 0.001$, $t_{(608)} = 6.206$) and multiple Brp rings (two rings close to each other) upon PhTx treatment (Fig. 5*C*, arrows). The ratio of Brp clusters containing multiple rings increased significantly from 4% in untreated control to 22% and 23% when GluR activity was blocked by PhTx for 10 and 30 min, respectively (Fig. 5*D*; $p < 0.001$, $t_{(25)} = 10.26$; $p < 0.001$, $t_{(18)} = 9.567$). Given that PhTx application induces a homeostatic increase in neurotransmitter release (Frank et al., 2006; Weyhersmüller et al., 2011), we hypothesized that multiple Brp rings may be correlated with the homeostatic increase in presynaptic release. To test this possibility, we performed SIM to examine the Brp staining in *GluRIIA*-null mutants, which also exhibit robust homeostatic regulation (Petersen et al., 1997; Davis and Goodman, 1998b). Compared with the WT, we found more clusters with multiple Brp rings in *GluRIIA*-null mutant boutons (Fig. 5*E,F*; $p < 0.001$, $t_{(24)} = 4.676$). Together, both pharmacological and genetic perturbations of GluRIIA similarly induced formation of multiple Brp rings at NMJ synapses.

Nlg1 mediates the formation of multiple Brp rings at *GluRIIC* NMJs

There are multiple “retrograde” signaling pathways from postsynaptic muscles to presynaptic motoneurons, which potentially mediate presynaptic homeostatic plasticity, such as BMP, TOR, CaMK II, Sem2B-PlexB, and cell adhesion molecules, such as integrin and N-Cadherins/ β -catenin. Still, a direct link between these signals and Brp intensity is unclear (Davis and Müller, 2015; Goel et al., 2017; Orr et al., 2017). Cell adhesion interactions mediated by Nlg1/Nrx-1 and Tenorins can control AZ morphology and structure (Li et al., 2007; Banovic et al., 2010; Mosca et al., 2012; Harris and Littleton, 2015). The level of Nlg1 at the synapse impacts NMJ size, and synaptic recruitment of Nlg1 is important for proper AZ scaffold assembly (Banovic et al., 2010). Furthermore, transsynaptic adhesion partners Nlg1 and Nrx-1 are im-

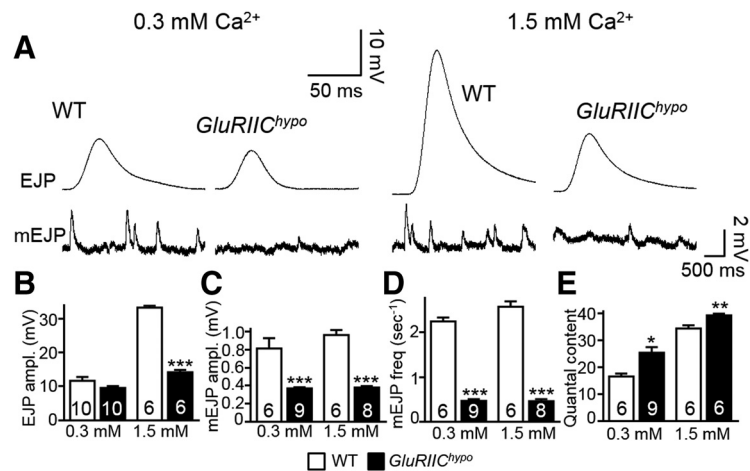


Figure 4. *GluRIIC* mutant NMJ synapses show homeostatic regulation. **A**, Representative EJP and spontaneous mEJP traces at NMJ synapses of WT and *GluRIIC*^{hypo} at 0.3 and 1.5 mM Ca²⁺. Scale bars for EJP and mEJP traces are annotated. **B–E**, Bar graphs of the EJP amplitude (**B**), mEJP amplitude (**C**), mEJP frequency (**D**), and QC (**E**) at 0.3 and 1.5 mM Ca²⁺ for WT and *GluRIIC*^{hypo} mutant. * $p < 0.05$, ** $p < 0.01$, *** $p < 0.001$. Error bars indicate SEM.

portant regulators of AZ morphology and apposition (Missler et al., 2012). Lack of GluRs recapitulates to some extent mutants in the Nlg1/Nrx-1 signaling pathway, which show fewer but larger and often misshapen AZs (Li et al., 2007; Banovic et al., 2010; Oswald et al., 2012). In contrast, lack of presynaptic Spinophilin (Spn), a protein phosphatase 1 binding protein, results in an opposite phenotype with more but smaller Brp rings, accompanied by increased levels of Nlg1/Nrx-1 (Muhammad et al., 2015). Based on the similar AZ phenotypes, we hypothesized that GluRs and Nlg1 might act together to regulate AZ scaffold structure.

To determine whether Nlg1 was involved in the formation of multiple Brp ring AZs, we examined Nlg1 staining intensity at NMJ terminals of WT, *nlg1* mutant (*nlg1*^{exc2.3/ex1.9}), *GluRIIC*^{RNAi}, *GluRIIC*^{hypo}, and *GluRIIC* *res* and found a significant decrease in the intensity of Nlg1 (normalized to HRP staining) at *GluRIIC*^{RNAi} and *GluRIIC*^{hypo} mutant NMJs compared with WT (Fig. 6*A–C*; $p < 0.001$ for both *GluRIIC*^{RNAi} and *GluRIIC*^{hypo}), indicating that GluRs may stabilize Nlg1 at NMJ synapses. The reduction of overall Nlg1 intensity is probably attributable to the reduced Nlg1 at individual AZs. In the most severe cases, the juxtaposition of Nlg1 with Brp puncta was lost (Fig. 6*A–C*); specifically, the percentage of AZs without adjacent Nlg1 puncta was increased at *GluRIIC*-deficient NMJs (Fig. 6*A–C*; WT: $2.08 \pm 1.27\%$; *GluRIIC*^{RNAi}: $12.08 \pm 1.54\%$, $p = 0.001$, $t_{(8)} = 5.008$; *GluRIIC*^{hypo}: $12.44 \pm 1.38\%$, $p = 0.0006$, $t_{(8)} = 5.530$; *GluRIIC* *res*: $1.08 \pm 0.66\%$). The dependence on GluRs for synaptic Nlg1 localization suggest that they might function together. To determine a potential role for Nlg1 in *GluRIIC* deficiency-induced AZ structural plasticity, we conducted genetic interaction analysis of *nlg1* and *GluRIIC* (Fig. 6*D,E*; Fig. 6-1, available at <https://doi.org/10.1523/JNEUROSCI.2002-19.2020.f6-1>). Reducing the dose of *nlg1* by half (*nlg1*^{exc2.3/+}) showed no detectable effect on Brp size (Fig. 6-1, available at <https://doi.org/10.1523/JNEUROSCI.2002-19.2020.f6-1>). However, there were similarly enlarged Brp puncta in *nlg1* mutants and *GluRIIC*^{+/+},*nlg1*^{+/+} double-heterozygotes (*GluRIIC*^{2/nlg1}^{exc2.3}) (Fig. 6*D*; Fig. 6-1, available at <https://doi.org/10.1523/JNEUROSCI.2002-19.2020.f6-1>). Knockdown of *GluRIIC* in *nlg1*^{exc2.3/ex1.9} background led to fewer and larger Brp puncta as in *GluRIIC*^{RNAi} and *GluRIIC*^{hypo} mutant NMJs (Fig. 6-1, available at <https://doi.org/10.1523/JNEUROSCI.2002-19.2020.f6-1>). Moreover, the Brp puncta size was reduced to the WT level upon

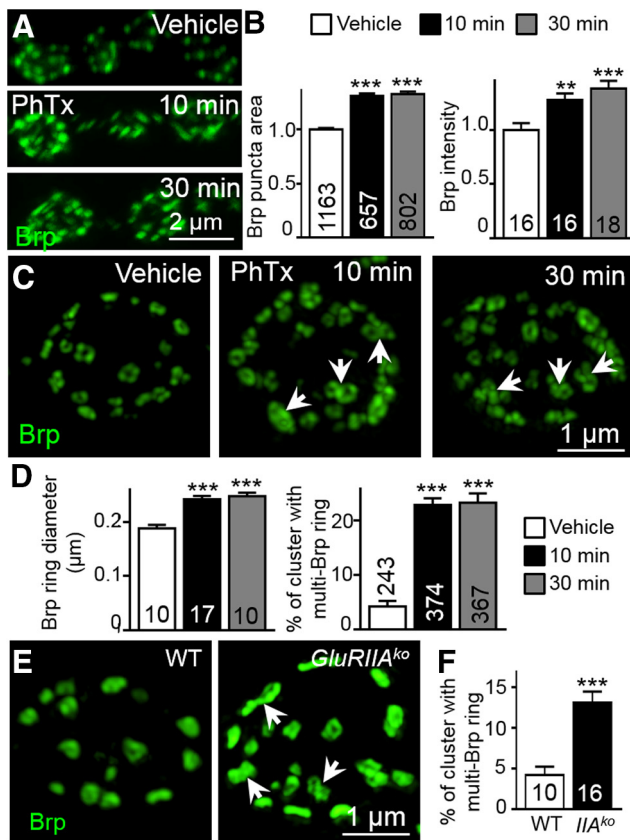


Figure 5. Acute inhibition of GluR activity by PhTx results in clustering of multiple Brp rings. **A**, Representative confocal images of different treatments (vehicle, 10 min with PhTx, and 30 min with PhTx) stained with anti-Brp (green). Scale bar, 2 μm. **B**, Bar graph represents the normalized area of Brp puncta (vehicle:10 min with PhTx:30 min with PhTx) and the normalized fluorescence intensity of anti-Brp staining at NMJs of different treatments (vehicle:10 min with PhTx:30 min with PhTx). **C**, SIM images of WT NMJ4 boutons stained with anti-Brp (green). Clusters of multiple Brp rings (arrows) increased when larvae were treated with PhTx for 10 min (middle) and 30 min (right) compared with the vehicle control (left). Scale bar, 1 μm. **D**, Quantification of the percentage of multiple Brp rings and Brp ring diameters in the vehicle control and PhTx-treated larvae NMJs. For diameter of single Brp ring at *GluRIIC* and *GluRIIA* mutant synapses, see also Figure 5-1 (available at <https://doi.org/10.1523/JNEUROSCI.2002-19.2020.f5-1>). **E**, SIM images of WT and *GluRIIA^{ko}* (*DfCh⁴/GluRIIA^{AD9}*) mutant boutons labeled with anti-Brp. Scale bar, 1 μm. **F**, Quantifications of the percentage of multiple Brp rings at WT and *GluRIIA* mutant boutons. ***p* < 0.01, ****p* < 0.001.

nlg1 overexpression in the *GluRIIC^{RNAi}* background (Fig. 6D,F; *p* = 0.0006, *t*₍₁₉₎ = 4.132), whereas *nlg1* overexpression in the WT background led to no detectable effect on Brp puncta (Fig. 6D,F).

Previous studies report that Nlg1, when overexpressed, is able to recruit postsynaptic proteins (Dlg and GluRIIC) to postsynaptic terminals (Banovic et al., 2010). Thus, we costained NMJ terminals with anti-GluRIIA (a major player in neurotransmission compared with GluRIIB) and anti-HRP to quantify postsynaptic GluRIIA in different genotypes. We found larger but fewer GluRIIA puncta (normalized to synaptic HRP area) when Nlg1-GFP was overexpressed in WT background (Fig. 6-3, available at <https://doi.org/10.1523/JNEUROSCI.2002-19.2020.f6-3>). When Nlg1-GFP was overexpressed in *GluRIIC^{RNAi}* background, we noticed a significant increase of GluRIIA puncta number (Fig. 6-3A,B, available at <https://doi.org/10.1523/JNEUROSCI.2002-19.2020.f6-3>; *p* = 0.0023, *t*₍₄₇₎ = 3.223). We found a significantly increased area of individual GluRIIA puncta when *nlg1* was overexpressed in WT but not *GluRIIC^{RNAi}* background (Fig. 6-3, available

at <https://doi.org/10.1523/JNEUROSCI.2002-19.2020.f6-3>). Together, these data show that *nlg1* overexpression partially restored the reduced number of GluRIIA puncta induced by *GluRIIC* RNAi knockdown.

SIM analysis confirmed that the enlarged Brp puncta in *nlg1* mutants consisted of multiple Brp rings, similar to that at *GluRIIC^{RNAi}* boutons (Fig. 6E). Importantly, the percentage of multiple Brp rings in *GluRIIC^{RNAi}* boutons was rescued by *nlg1* overexpression (Fig. 6E,G). These results suggest that GluRs and Nlg1 cooperated in controlling the formation of multiple Brp rings.

Because of the rescue of the increased percentage of multiple Brp ring phenotype in *GluRIIC* RNAi knockdown by *nlg1* overexpression (Fig. 6E,G), we performed a physiological assay to test whether *nlg1* overexpression could rescue the reduced neurotransmission in *GluRIIC^{RNAi}* synapses. We recorded EJP and mEJP at 1.0 mM extracellular calcium at the larval NMJs of different genotypes, including WT, *GluRIIC^{RNAi}*, *nlg1* overexpression (*UAS-nlg1-GFP/+;C57-Gal4/+*), and *nlg1* overexpression at the *GluRIIC^{RNAi}* background (*UAS-nlg1-GFP/+;C57-Gal4, GluRIIC^{RNAi}/+*) (Fig. 7A). Postsynaptic overexpression of *nlg1* by *C57-Gal4* in the WT background showed similar neurotransmission as the WT (Fig. 7A–E). However, postsynaptic overexpression of *nlg1* partially rescued the reduced mEJP amplitudes (*p* < 0.001, *t*₍₁₃₎ = 6.814) and mEJP frequency (*p* < 0.001, *t*₍₂₆₎ = 6.604) but not EJP amplitudes (*p* = 0.068, *t*₍₁₃₎ = 1.989) of *GluRIIC^{RNAi}* (Fig. 7A–D), consistent with the recruitment of GluRIIA described above (Fig. 6-3, available at <https://doi.org/10.1523/JNEUROSCI.2002-19.2020.f6-3>). The increased QC in *GluRIIC^{RNAi}* was also partially reduced by *nlg1* overexpression (Fig. 7E; *p* = 0.0312, *t*₍₁₇₎ = 2.348). As *nlg1* overexpression rescued the structural and functional synapse phenotypes associated with GluR reduction, it was likely that Nlg1 was a downstream effector of GluRs in regulating presynaptic AZ formation.

Thus, Nlg1 might play a permissive role in the formation of presynaptic multiple Brp rings induced by reduced glutamate receptors. To clarify whether *nlg1* itself was required for synaptic homeostasis, we performed physiological assays with PhTx. Our data show that *nlg1* mutant NMJs exhibited no PHP (Fig. 7; Fig. 7-1, available at <https://doi.org/10.1523/JNEUROSCI.2002-19.2020.f7-1>). As shown in Figure 7-1D, F (available at <https://doi.org/10.1523/JNEUROSCI.2002-19.2020.f7-1>), both EJP and QC were decreased at the *nlg1* mutant NMJ synapses compared with the WT. Upon treatment of PhTx, we observed decreased mEJP amplitude but no increase in QC in *nlg1* mutants compared with pre-treated controls (Fig. 7-1, available at <https://doi.org/10.1523/JNEUROSCI.2002-19.2020.f7-1>). Thus, loss of *nlg1* does not induce presynaptic homeostasis, suggesting that Nlg1 is normally involved in the homeostatic regulation.

Discussion

Synaptic homeostasis is a fundamental mechanism to maintain efficient neurotransmission of the neural network. At the *Drosophila* peripheral NMJ, each AZ usually contains a single T-bar. Here, we report multiple T-bars at a single AZ apposed with the remaining GluRs when GluRs are reduced. Separate from formation of multiple T-bars, there are other strategies to enhance presynaptic transmitter release (i.e., by increasing Ca²⁺ channels and action potential-induced Ca²⁺ influx and by an increase in the size of readily releasable pool) (Weyhermüller et al., 2011; Davis and Müller, 2015; Gratz et al., 2019). Recently, Böhme et al. (2019) showed by STED microscopy that, within enlarged individual Brp rings, there are more “nano-clusters” per

Brp ring upon PhTx treatment. Based on structural and functional studies on *GluRIIC* mutants as well as classical PHP paradigms, we propose that multiple T-bars are associated with synaptic homeostasis, although the biological significance of multiple T-bars is not clear at the moment.

Multiple Brp rings are associated with homeostatic regulation

Homeostatic regulation has been observed upon genetic loss and pharmacological blockage of GluRIIA (Petersen et al., 1997; Frank et al., 2006; Davis and Müller, 2015; Goel et al., 2017). Acute pharmacological blockage of receptors by PhTx reduces mEJP amplitude, initiating rapid increases in QC within 10 min (Frank et al., 2006; Davis and Müller, 2015). Similarly, *GluRIIA* mutants exhibit a large decrease in mEJP amplitudes with no change in EJP amplitudes, indicating a compensatory increase in QC (Petersen et al., 1997). At *GluRIIC* mutant NMJs, we showed a significant reduction in mEJP amplitude accompanied with an increase in QC (i.e., synaptic efficacy), but a normal EJP amplitude, at least at a low level of calcium, indicative of homeostatic regulation (Fig. 4).

In PhTx-treated animals and *GluRIIA* mutants, the intensity of the AZ protein Brp and the number of release-ready vesicles increase during homeostatic regulation (Weyhersmüller et al., 2011). In addition, increased number and density of T-bars were observed in *GluRIIA* mutants (Reiff et al., 2002). Consistently, we observed an increased Brp intensity and multiple Brp rings at the NMJs of *GluRIIC* mutants (Figs. 1A, 2A). Similarly, we showed that the NMJ synapses of both PhTx-treated and *GluRIIA* mutant larvae exhibited multiple Brp rings as in *GluRIIC* mutants (Fig. 5C,E). Thus, the formation of multiple Brp rings at AZs may be the structural basis of synaptic homeostasis, at least for GluR-associated homeostatic regulation.

We observed apparent multiple Brp rings at the NMJ boutons of *GluRIIA* or *GluRIIC* mutants as well as PhTx-treated animals (Figs. 2A, 5E). However, there are differences in the structural changes of the Brp ring in different genotypes or upon different treatments. For example, individual Brp rings enlarged at PhTx-treated, but not in *GluRIIA* and *GluRIIC* mutant NMJ synapses (Fig. 5D; Fig. 5-1A,B, available at <https://doi.org/10.1523/JNEUROSCI.2002-19.2020.f5-1>). The number of Brp rings in Brp cluster was also different; two

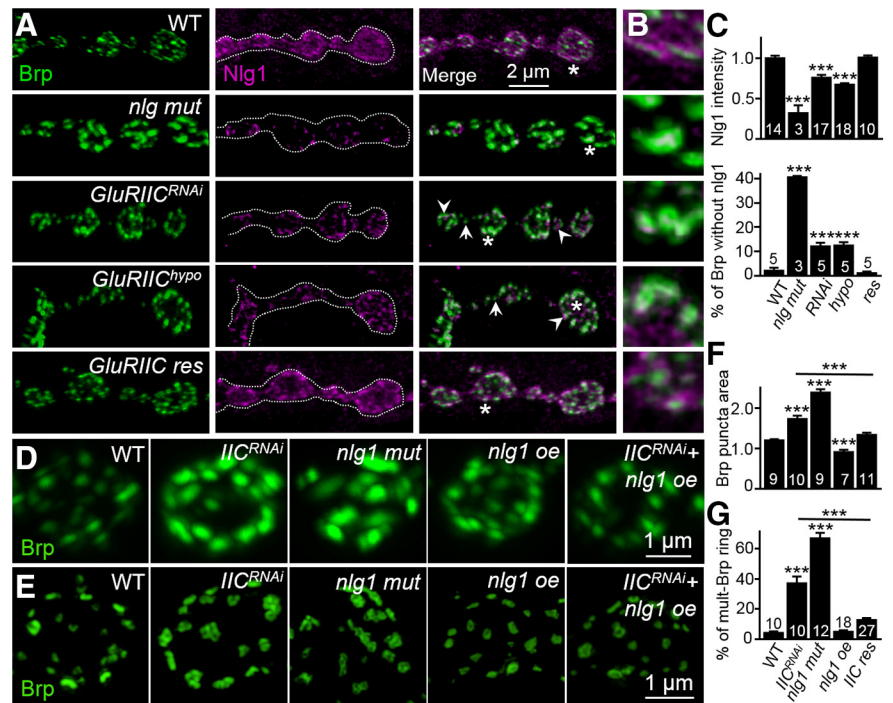


Figure 6. Overexpression of *nlg1* rescues the phenotype of multiple Brp rings of *GluRIIC* mutants. **A**, Representative confocal images of synaptic boutons costained with anti-Brp (green) and anti-Nlg1 (magenta) in the WT, *nlg1* mutant (*nlg1^{ex2.3/ex1.9}*), *GluRIIC^{RNAi}* (*C57-Gal4/GluRIIC^{RNAi}*), *GluRIIC^{hyppo}* (*GluRIIC²/Dfast2; UAS-GluRIIC/+*), and *GluRIIC^{res}* (*GluRIIC²/Dfast2;GluRIIC/+*). Arrows indicate Brp puncta without adjacent Nlg1 staining. Arrowheads indicate the Brp puncta with adjacent Nlg1. Scale bar, 2 μ m. Nr1 staining at NMJs expressing reduced GluRs is shown in Figure 6-2 (available at <https://doi.org/10.1523/JNEUROSCI.2002-19.2020.f6-2>). **B**, Higher-magnification images of Brp and Nlg1 staining of a single synapse in **A** (asterisks). **C**, Quantification of Nlg1 normalized staining intensity and the percentage of Brp puncta without Nlg1 staining in different genotypes. **D**, Higher-magnification images of NMJ boutons from different genotypes stained with anti-Brp (green). The five genotypes are WT, *GluRIIC^{RNAi}*, *nlg1* mutant (*nlg1^{ex2.3/ex1.9}*), *nlg1* overexpression (oe) (*UAS-nlg1-GFP/+;C57-Gal4/+*), and *GluRIIC^{RNAi}+nlg1* oe (*UAS-nlg1-GFP/+;C57-Gal4,GluRIIC^{RNAi}+nlg1*). Scale bar, 1 μ m. For genetic interaction analysis between *GluRIIC* and *nlg1* in regulating Brp puncta area, see also Figure 6-1 (available at <https://doi.org/10.1523/JNEUROSCI.2002-19.2020.f6-1>). **E**, SIM images of Brp rings at single NMJ boutons of different genotypes. There are multiple Brp ring clusters in *nlg1* mutant boutons, similar to that in *GluRIIC^{RNAi}* boutons. *nlg1* overexpression rescues the multiple Brp ring clusters in *GluRIIC^{RNAi}*. Scale bar, 1 μ m. For rescue of GluRIIA expression at *GluRIIC^{RNAi}* NMJs by overexpressed *nlg1*, see also Figure 6-3 (available at <https://doi.org/10.1523/JNEUROSCI.2002-19.2020.f6-3>). **F, G**, Quantification of normalized individual Brp puncta area (**F**) and percentage of multiple Brp rings (**G**) at NMJ boutons of different genotypes. Error bars indicate SEM. ns, $p > 0.05$; * $p < 0.05$; *** $p < 0.001$.

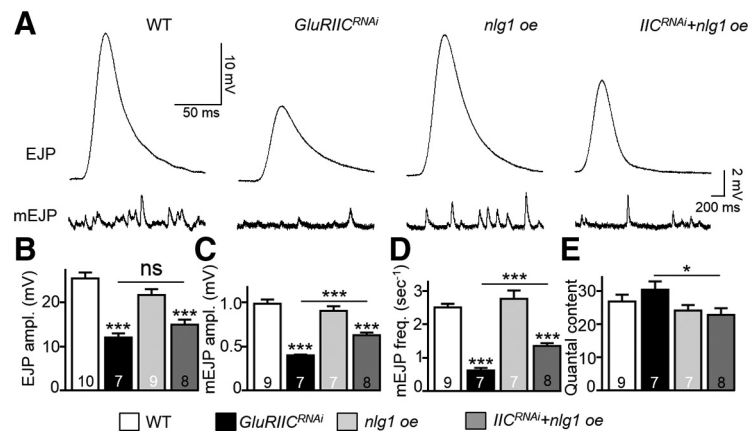


Figure 7. Overexpression of *nlg1* partially rescues reduced neurotransmission of *GluRIIC* mutants. **A**, Representative EJP and mEJP traces of WT, *GluRIIC^{RNAi}* (*C57-Gal4/GluRIIC^{RNAi}*), *nlg1* oe (*UAS-nlg1-GFP/+;C57-Gal4/+*), and *GluRIIC^{RNAi}+nlg1* oe (*UAS-nlg1-GFP/+;C57-Gal4,GluRIIC^{RNAi}+nlg1*). The scale bars for EJP and mEJP traces are annotated. For *nlg1* mutant treated with PhTx, see also Figure 7-1 (available at <https://doi.org/10.1523/JNEUROSCI.2002-19.2020.f7-1>). **B–E**, Histogram showing EJP amplitudes (**B**), mEJP amplitude (**C**), mEJP frequency (**D**), and QC (**E**) for different genotypes. *GluRIIC* mutants showed decreased EJP amplitudes, mEJP amplitudes, and mEJP frequency of synaptic transmission. *nlg1* overexpression partially rescued the reduced neurotransmission in *GluRIIC^{RNAi}*. Error bars indicate SEM. ns, $p > 0.05$; * $p < 0.05$; *** $p < 0.001$.

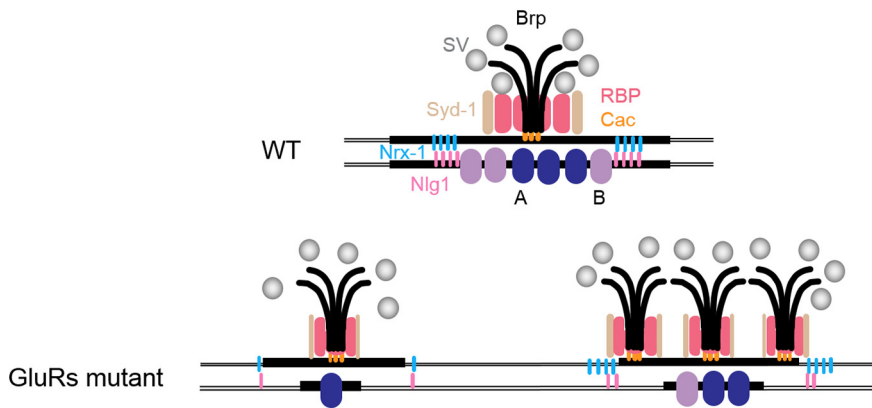


Figure 8. Model describing the role of Nlg1/Nrx in controlling the formation of multiple T-bars at *GluRIIC* mutant NMJs. At WT NMJ synapses, there is one T-bar per AZ. When GluRs are reduced, cell adhesion molecule Nlg1 is reduced and preferentially localized to enlarged Brp puncta at NMJ synapses. AZs juxtaposed with preferentially enriched GluRs and adjacent Nlg1 usually have multiple T-bars, whereas AZs with few GluRs and no adjacent Nlg1 tend to have single T-bars at *GluRIIC* mutant NMJs. A, *GluRIIA*; B, *GluRIIB*. Thick black bar across *GluRIIA* and *IIB* represents PSD.

adjacent Brp rings were mostly observed in *GluRIIA* and PhTx-treated NMJ synapses (Fig. 5C,E), but Brp clusters with 2–5 rings were observed in *GluRIIC* mutant NMJs (Fig. 2F). Clusters of Brp rings formed minutes after PhTx treatment, suggesting that synaptic homeostasis may occur locally and acutely involve rapid mobilization of synaptic materials to the AZs (Goel et al., 2019; Gratz et al., 2019) without transcriptional regulation, consistent with previous findings that AZs are remarkably plastic and their protein composition can be rapidly and reversibly modified (Graf et al., 2009; Böhme et al., 2016). However, transcriptional and translational regulation might be involved in the formation of multiple Brp rings in the timescale of days when *GluRIIA* or *GluRIIC* was genetically disrupted.

Our data as well as independent findings from the literature firmly established that AZ materials are increased during PHP (Weyhersmüller et al., 2011; Böhme et al., 2019; Goel et al., 2019; Gratz et al., 2019) (Fig. 5). However, Goel et al. (2019) reported that homeostatic increases in QC can be uncoupled from AZ enhancements during an acute induction of PHP using PhTx in the mutant NMJs of *arl8*, which encodes a lysosomal kinesin adaptor (Goel et al., 2019). We also found significantly increased Brp puncta but no PHP detected in *nlg1* mutants (Fig. 7-1, available at <https://doi.org/10.1523/JNEUROSCI.2002-19.2020.f7-1>). Thus, enlarged Brp puncta does not underlie but associate with synaptic homeostasis.

Studies in mammals have found that AZ proteins are dynamic and subject to homeostatic regulation over both acute and chronic timescales (Glebov, 2017; Thalhammer et al., 2017; Hruska et al., 2018). For example, recent work using multicolor STED microscopy identified AZ nano-modules containing Bassoon, vGluT, and synaptophysin and revealed a linear scaling of the number of these nano-modules with spine volume upon chemically induced LTP (Hruska et al., 2018). AZ structure is also tightly regulated by neuronal activity; long-term blockade of neuronal activity leads to reversible AZ matrix unclustering, whereas stimulation of postsynaptic neurons retrogradely enhances clustering of AZ proteins (Glebov et al., 2017). Together, extensive recent studies in *Drosophila* and mammals demonstrate that structural reorganization of AZs is a conserved mechanism for modulating neurotransmission efficacy.

Decreased Nlg1/Nrx-1 signaling mediates multiple Brp ring formation

How do multiple T-bars form in *GluRIIC* mutants? We propose that multiple T-bar formation might be a functional compensation of reduced neurotransmission at *GluRIIC*-deficient NMJs and that trans-synaptic Nlg1/Nrx-1 cell adhesion signaling may mediate the homeostatic plasticity induced by reduced GluRs (Fig. 8). At the molecular level, Nrx-1 molecules get stabilized at the presynaptic membrane by an interaction with the PDZ domain of Syd-1. Syd-1/Liprin- α complex then initiates AZ formation characterized by Brp recruitment (Owald et al., 2012). Spinophilin acts antagonistically to Syd-1. Specifically, Spn competes with Syd-1 to bind Nrx-1 with its PDZ domain, thus reducing the amount of Nrx-1 available for Syd-1 binding (Muhammad et al., 2015).

Loss of presynaptic Spn results in the formation of excess, but atypically small AZs, opposite to that in *GluRIIC* mutants. Nlg1/Nrx-1/Syd-1 levels are increased at *spn* mutant NMJs, and removal of a copy of *nrx-1*, *Syd-1*, or *nlg1* genes suppresses the *spn* AZ phenotype (Muhammad et al., 2015). Thus, the interactions among Nlg1/Nrx-1/Syd-1 help control the seeding and ultimately the number of AZs at a presynaptic bouton.

Once Nrx-1 is anchored at the presynaptic membrane, it forms a bridge with its postsynaptic partner Nlg1. In this way, trans-synaptic contact can also initiate postsynaptic scaffold assembly, mainly incorporation of GluRs into the postsynaptic densities. Formation of postsynaptic Nlg1 puncta depends on presynaptic Nrx-1. However, Nrx-1 binding is not absolutely required for Nlg1 function (Banovic et al., 2010). It is not known how presynaptic Nrx-1 acts when postsynaptic Nlg1 is reduced. When *GluRIIC* was mutated, Nlg1 was reduced and mislocalized (Fig. 6A–C). Different from reduced Nlg1, Nrx-1 puncta size instead increased significantly, in conjunction with increased Brp and Syd-1 puncta in *GluRIIC* mutant NMJs, compared with WT (Fig. 1-1A–D, available at <https://doi.org/10.1523/JNEUROSCI.2002-19.2020.f1-1>; Fig. 6-2, available at <https://doi.org/10.1523/JNEUROSCI.2002-19.2020.f6-2>). In contrast to the more and smaller AZs in *spn* mutant NMJ, we observed fewer and larger AZs with multiple Brp rings in *GluRIIC* mutants (Fig. 1). We speculated that the formation of multiple Brp rings at AZs, which have higher release probabilities, may be a functional compensation effect for the reduced synaptic transmission in *GluRIIC* mutant. The compromised interactions between Nlg1 with Nrx-1 may, directly or indirectly, lead to the remaining GluRs preferentially juxtaposed to the AZs with multiple Brp rings. This notion is supported by previous studies of both anatomical and physiological analysis demonstrating that GluRs preferentially cluster opposite larger Brp-positive AZs (Marrus et al., 2004; Graf et al., 2009).

As multiple Brp rings are a prominent structure at presynaptic terminals induced by homeostatic regulation and synaptic homeostasis is an important and well-conserved process, it will be of great interest to further elucidate the molecular mechanisms by which multiple Brp rings form during homeostatic regulation at synapses and to clarify the functional implication of multiple Brp rings in PHP.

References

- Banovic D, Khorramshahi O, Oswald D, Wichmann C, Riedt T, Fouquet W, Tian R, Sigrist SJ, Aberle H (2010) *Drosophila* neuroligin 1 promotes growth and postsynaptic differentiation at glutamatergic neuromuscular junctions. *Neuron* 66:724–738.
- Böhme MA, Beis C, Reddy-Alla S, Reynolds E, Mampell MM, Grasskamp AT, Lützkendorf J, Bergeron DD, Driller JH, Babikir H, Göttfert F, Robinson IM, O’Kane CJ, Hell SW, Wahl MC, Stelzl U, Loll B, Walter AM, Sigrist SJ (2016) Active zone scaffolds differentially accumulate Unc13 isoforms to tune Ca²⁺ channel-vesicle coupling. *Nat Neurosci* 19:1311–1320.
- Böhme MA, McCarthy AW, Grasskamp AT, Beuschel CB, Goel P, Jusyte M, Laber D, Huang S, Rey U, Petzoldt AG, Lehmann M, Göttfert F, Haghghi P, Hell SW, Oswald D, Dickman D, Sigrist SJ, Walter AM (2019) Rapid active zone remodeling consolidates presynaptic potentiation. *Nat Commun* 10:1085.
- Cull-Candy SG, Miledi R, Trautmann A, Uchitel OD (1980) On the release of transmitter at normal, myasthenia gravis and myasthenic syndrome affected human end-plates. *J Physiol* 299:621–638.
- Dai Y, Taru H, Deken SL, Grill B, Ackley B, Nonet ML, Jin Y (2006) SYD-2 liprin- α organizes presynaptic active zone formation through ELKS. *Nat Neurosci* 9:1479–1487.
- Dalva MB, McClelland AC, Kayser MS (2007) Cell adhesion molecules: signalling functions at the synapse. *Nat Rev Neurosci* 8:206–220.
- Davis GW, Goodman CS (1998a) Genetic analysis of synaptic development and plasticity: homeostatic regulation of synaptic efficacy. *Curr Opin Neurobiol* 8:149–156.
- Davis GW, Goodman CS (1998b) Synapse-specific control of synaptic efficacy at the terminals of a single neuron. *Nature* 392:82–86.
- Davis GW, Müller M (2015) Homeostatic control of presynaptic neurotransmitter release. *Annu Rev Physiol* 77:251–270.
- DiAntonio A, Petersen SA, Heckmann M, Goodman CS (1999) Glutamate receptor expression regulates quantal size and quantal content at the *Drosophila* neuromuscular junction. *J Neurosci* 19:3023–3032.
- Featherstone DE, Rushton E, Rohrbough J, Liebl F, Karr J, Sheng Q, Rodesch CK, Brodie K (2005) An essential *Drosophila* glutamate receptor subunit that functions in both central neuropil and neuromuscular junction. *J Neurosci* 25:3199–3208.
- Fouquet W, Oswald D, Wichmann C, Mertel S, Depner H, Dyba M, Hallermann S, Kittel RJ, Eimer S, Sigrist SJ (2009) Maturation of active zone assembly by *Drosophila* bruchpilot. *J Cell Biol* 186:129–145.
- Frank CA, Kennedy MJ, Goold CP, Marek KW, Davis GW (2006) Mechanisms underlying the rapid induction and sustained expression of synaptic homeostasis. *Neuron* 52:663–677.
- Giagtzoglou N, Mahoney T, Yao CK, Bellen HJ (2009) Rab3 GTPase lands bruchpilot. *Neuron* 64:595–597.
- Glebov OO, Jackson RE, Winterflood CM, Owen DM, Barker EA, Doherty P, Ewers H, Burrone J (2017) Nanoscale structural plasticity of the active zone matrix modulates presynaptic function. *Cell Rep* 18:2715–2728.
- Goel P, Li X, Dickman D (2017) Disparate postsynaptic induction mechanisms ultimately converge to drive the retrograde enhancement of presynaptic efficacy. *Cell Rep* 21:2339–2347.
- Goel P, Dufour Bergeron D, Böhme MA, Nunnally L, Lehmann M, Buser C, Walter AM, Sigrist SJ, Dickman D (2019) Homeostatic scaling of active zone scaffolds maintains global synaptic strength. *J Cell Biol* 5:1706–1724.
- Goold CP, Davis GW (2007) The BMP ligand gbb gates the expression of synaptic homeostasis independent of synaptic growth control. *Neuron* 56:109–123.
- Graf ER, Daniels RW, Burgess RW, Schwarz TL, DiAntonio A (2009) Rab3 dynamically controls protein composition at active zones. *Neuron* 64:663–677.
- Gratz SJ, Goel P, Bruckner JJ, Hernandez RX, Khateeb K, Macleod GT, Dickman D, O’Connor-Giles KM (2019) Endogenous tagging reveals differential regulation of Ca(2+) channels at single active zones during presynaptic homeostatic potentiation and depression. *J Neurosci* 39:2416–2429.
- Gustafsson MG, Shao L, Carlton PM, Wang CJ, Golubovskaya IN, Cande WZ, Agard DA, Sedat JW (2008) Three-dimensional resolution doubling in wide-field fluorescence microscopy by structured illumination. *Biophys J* 94:4957–4970.
- Haghghi AP, McCabe BD, Fetter RD, Palmer JE, Hom S, Goodman CS (2003) Retrograde control of synaptic transmission by postsynaptic CaMKII at the *Drosophila* neuromuscular junction. *Neuron* 39:255–267.
- Harris KP, Littleton JT (2015) Transmission, development, and plasticity of synapses. *Genetics* 201:345–375.
- Harris KP, Zhang YV, Piccioli ZD, Perrimon N, Littleton JT (2016) The postsynaptic t-SNARE Syntaxin 4 controls traffic of Neuroligin 1 and Synaptotagmin 4 to regulate retrograde signaling. *Elife* 5:e13881.
- Hruska M, Henderson N, Le Marchand SJ, Jafri H, Dalva MB (2018) Synaptic nanomodules underlie the organization and plasticity of spine synapses. *Nat Neurosci* 21:671–682.
- Kittel RJ, Wichmann C, Rasse TM, Fouquet W, Schmidt M, Schmid A, Wagh DA, Pawlu C, Kellner RR, Willig KI, Hell SW, Buchner E, Heckmann M, Sigrist SJ (2006) Bruchpilot promotes active zone assembly, Ca²⁺ channel clustering, and vesicle release. *Science* 312:1051–1054.
- Li J, Ashley J, Budnik V, Bhat MA (2007) Crucial role of *Drosophila* neuroligin in proper active zone apposition to postsynaptic densities, synaptic growth, and synaptic transmission. *Neuron* 55:741–755.
- Liu KS, Siebert M, Mertel S, Knoche E, Wegener S, Wichmann C, Matkovic T, Muhammad K, Depner H, Mettke C, Bückers J, Hell SW, Müller M, Davis GW, Schmitz D, Sigrist SJ (2011) RIM-binding protein, a central part of the active zone, is essential for neurotransmitter release. *Science* 334:1565–1569.
- Marrus SB, DiAntonio A (2004) Preferential localization of glutamate receptors opposite sites of high presynaptic release. *Curr Biol* 14:924–931.
- Marrus SB, Portman SL, Allen MJ, Moffat KG, DiAntonio A (2004) Differential localization of glutamate receptor subunits at the *Drosophila* neuromuscular junction. *J Neurosci* 24:1406–1415.
- Matkovic T, Siebert M, Knoche E, Depner H, Mertel S, Oswald D, Schmidt M, Thomas U, Sickmann A, Kamin D, Hell SW, Bürger J, Hollmann C, Mielke T, Wichmann C, Sigrist SJ (2013) The bruchpilot cytomatrix determines the size of the readily releasable pool of synaptic vesicles. *J Cell Biol* 202:667–683.
- McCabe BD, Marqués G, Haghghi AP, Fetter RD, Crotty ML, Haerry TE, Goodman CS, O’Connor MB (2003) The BMP homolog gbb provides a retrograde signal that regulates synaptic growth at the *Drosophila* neuromuscular junction. *Neuron* 39:241–254.
- Missler M, Südhof TC, Biederer T (2012) Synaptic cell adhesion. *Cold Spring Harb Perspect Biol* 4:a005694.
- Mosca TJ, Hong W, Dani VS, Favaloro V, Luo L (2012) Trans-synaptic teneurin signalling in neuromuscular synapse organization and target choice. *Nature* 484:237–241.
- Muhammad K, Reddy-Alla S, Driller JH, Schreiner D, Rey U, Böhme MA, Hollmann C, Ramesh N, Depner H, Lutzkendorf J, Lützkendorf J, Matkovic T, Götz T, Bergeron DD, Schmoranzler J, Goettfert F, Holt M, Wahl MC, Hell SW, Scheiffele P, et al. (2015) Presynaptic spinophilin tunes neuroligin signalling to control active zone architecture and function. *Nat Commun* 6:8362.
- Müller M, Pym EC, Tong A, Davis GW (2011) Rab3-GAP controls the progression of synaptic homeostasis at a late stage of vesicle release. *Neuron* 69:749–762.
- Orr BO, Fetter RD, Davis GW (2017) Retrograde semaphorin-plexin signalling drives homeostatic synaptic plasticity. *Nature* 550:109–113.
- Oswald D, Fouquet W, Schmidt M, Wichmann C, Mertel S, Depner H, Christiansen F, Zube C, Quentin C, Körner J, Urlaub H, Mechtler K, Sigrist SJ (2010) A syd-1 homologue regulates pre- and postsynaptic maturation in *Drosophila*. *J Cell Biol* 188:565–579.
- Oswald D, Khorramshahi O, Gupta VK, Banovic D, Depner H, Fouquet W, Wichmann C, Mertel S, Eimer S, Reynolds E, Holt M, Aberle H, Sigrist SJ (2012) Cooperation of syd-1 with neuroligin synchronizes pre- with postsynaptic assembly. *Nat Neurosci* 15:1219–1226.
- Peled ES, Newman ZL, Isacoff EY (2014) Evoked and spontaneous transmission favored by distinct sets of synapses. *Curr Biol* 24:484–493.
- Penney J, Tsurudome K, Liao EH, Elazzouzi F, Livingstone M, Gonzalez M, Sonenberg N, Haghghi AP (2012) TOR is required for the retrograde regulation of synaptic homeostasis at the *Drosophila* neuromuscular junction. *Neuron* 74:166–178.
- Petersen SA, Fetter RD, Noordermeer JN, Goodman CS, DiAntonio A (1997) Genetic analysis of glutamate receptors in *Drosophila* reveals a retrograde signal regulating presynaptic transmitter release. *Neuron* 19:1237–1248.
- Pilgram GS, Potikanond S, van der Plas MC, Fradkin LG, Noordermeer JN (2011) The RhoGAP crossveinless-c interacts with dystrophin and is required for synaptic homeostasis at the *Drosophila* neuromuscular junction. *J Neurosci* 31:492–500.

- Pozo K, Goda Y (2010) Unraveling mechanisms of homeostatic synaptic plasticity. *Neuron* 66:337–351.
- Qin G, Schwarz T, Kittel RJ, Schmid A, Rasse TM, Kappei D, Ponimaskin E, Heckmann M, Sigrist SJ (2005) Four different subunits are essential for expressing the synaptic glutamate receptor at neuromuscular junctions of *Drosophila*. *J Neurosci* 25:3209–3218.
- Rasse TM, Fouquet W, Schmid A, Kittel RJ, Mertel S, Sigrist CB, Schmidt M, Guzman A, Merino C, Qin G, Quentin C, Madeo FF, Heckmann M, Sigrist SJ (2005) Glutamate receptor dynamics organizing synapse formation in vivo. *Nat Neurosci* 8:898–905.
- Reiff DF, Thiel PR, Schuster CM (2002) Differential regulation of active zone density during long-term strengthening of *Drosophila* neuromuscular junctions. *J Neurosci* 22:9399–9409.
- Spiwok-Becker I, Glas M, Lasarzik I, Vollrath L (2004) Mouse photoreceptor synaptic ribbons lose and regain material in response to illumination changes. *Eur J Neurosci* 19:1559–1571.
- Sugie A, Hakeda-Suzuki S, Suzuki E, Silies M, Shimozone M, Möhl C, Suzuki T, Tavasani G (2015) Molecular remodeling of the presynaptic active zone of *Drosophila* photoreceptors via activity-dependent feedback. *Neuron* 86:711–725.
- Thalhammer A, Contestabile A, Ermolyuk YS, Ng T, Volynski KE, Soong TW, Goda Y, Cingolani LA (2017) Alternative splicing of P/Q-type Ca(2+) channels shapes presynaptic plasticity. *Cell Rep* 20:333–343.
- Turrigiano G (2012) Homeostatic synaptic plasticity: local and global mechanisms for stabilizing neuronal function. *Cold Spring Harb Perspect Biol* 4:a005736.
- Ullrich A, Böhme MA, Schöneberg J, Depner H, Sigrist SJ, Noé F (2015) Dynamical organization of syntaxin-1A at the presynaptic active zone. *PLoS Comput Biol* 11:e1004407.
- Wagh DA, Rasse TM, Asan E, Hofbauer A, Schwenkert I, Dürrbeck H, Buchner S, Dabauvalle MC, Schmidt M, Qin G, Wichmann C, Kittel R, Sigrist SJ, Buchner E (2006) Bruchpilot, a protein with homology to ELKS/CAST, is required for structural integrity and function of synaptic active zones in *Drosophila*. *Neuron* 49:833–844.
- Wang X, Wang Q, Engisch KL, Rich MM (2010) Activity-dependent regulation of the binomial parameters p and n at the mouse neuromuscular junction in vivo. *J Neurophysiol* 104:2352–2358.
- Wang X, Pinter MJ, Rich MM (2016) Reversible recruitment of a homeostatic reserve pool of synaptic vesicles underlies rapid homeostatic plasticity of quantal content. *J Neurosci* 36:828–836.
- Weyhermüller A, Hallermann S, Wagner N, Eilers J (2011) Rapid active zone remodeling during synaptic plasticity. *J Neurosci* 31:6041–6052.
- Zhai RG, Bellen HJ (2004) The architecture of the active zone in the presynaptic nerve terminal. *Physiology* 19:262–270.
- Zhao L, Wang D, Wang Q, Rodal AA, Zhang YQ (2013) *Drosophila* cyfip regulates synaptic development and endocytosis by suppressing filamentous actin assembly. *PLoS Genet* 9:e1003450.